Volume 6 | Number 24 | 21 December 2014 | Pages 14577–15348

Nanoscale

www.rsc.org/nanoscale

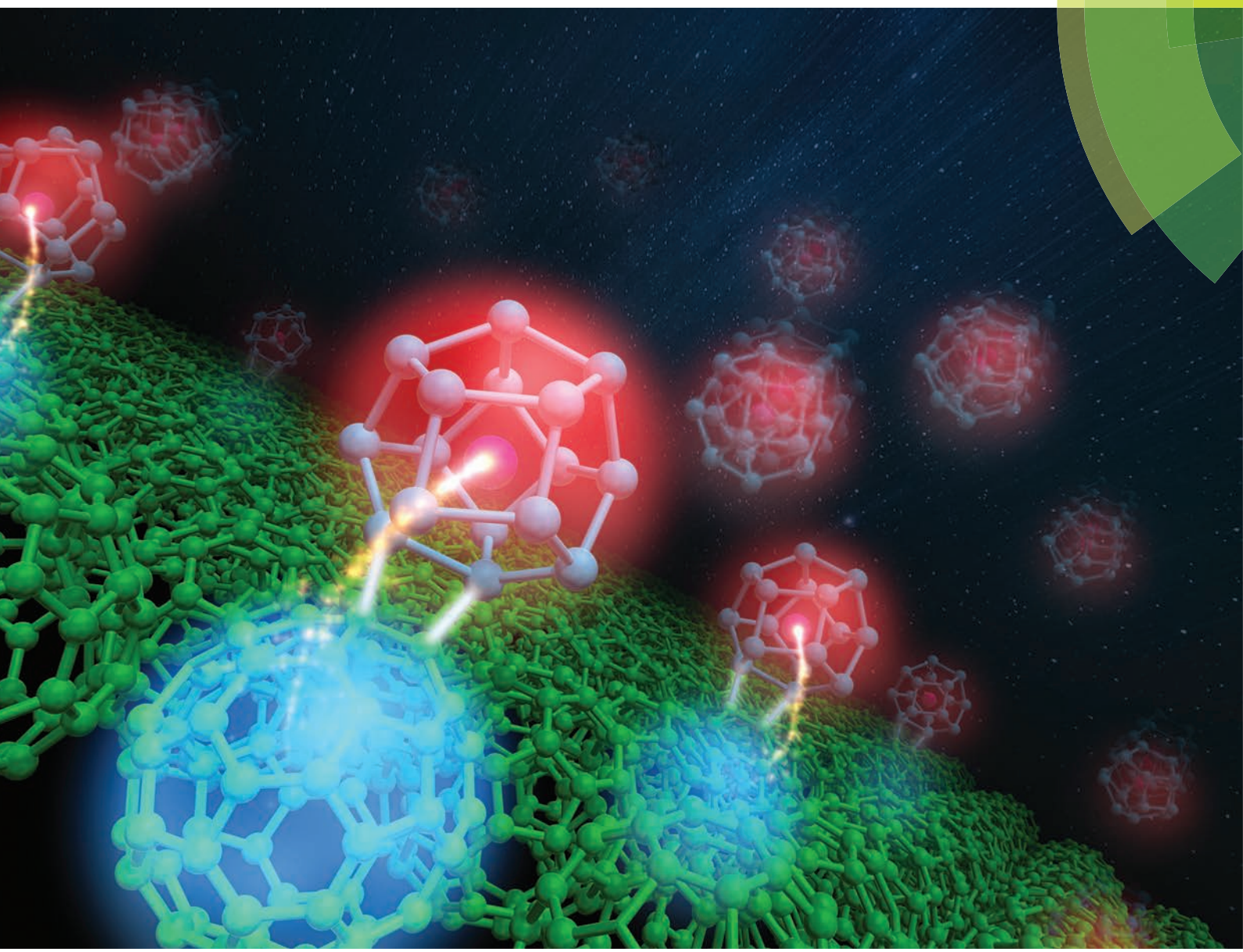

ISSN 2040-3364

ROYAL SOCIETY OF CHEMISTRY

PAPER
Atsushi Nakajima *et al.*
Formation of a superatom monolayer using gas-phase-synthesized $Ta@Si_{16}$ nanocluster ions

NCNST

Nanoscale

PAPER

View Article Online
View Journal | View Issue

Cite this: *Nanoscale*, 2014, **6**, 14702

Formation of a superatom monolayer using gas-phase-synthesized Ta@Si_{16} nanocluster ions†

Masato Nakaya,[a,b] Takeshi Iwasa,[a,b] Hironori Tsunoyama,[a,b] Toyoaki Eguchi[a,b] and Atsushi Nakajima*[a,b,c]

Received 25th July 2014,
Accepted 8th September 2014

DOI: 10.1039/c4nr04211e

www.rsc.org/nanoscale

The controlled assembly of superatomic nanocluster ions synthesized in the gas phase is a key technology for constructing a novel series of functional nanomaterials. However, it is generally difficult to immobilize them onto a conductive surface while maintaining their original properties owing to undesirable modifications of their geometry and charge state. In this study, it has been shown that this difficulty can be overcome by controlling the donor–acceptor interaction between nanoclusters and surfaces. Cations of Ta-atom-encapsulated Si_{16} cage nanoclusters (Ta@Si_{16}) behaving as rare-gas-like superatoms are synthesized in the gas phase and deposited on conductive surfaces terminated with acceptor-like C_{60} and donor-like α-sexithiophene (6T) molecules. Scanning tunneling microscopy and spectroscopy have demonstrated that Ta@Si_{16} cations can be densely immobilized onto C_{60}-terminated surfaces while retaining their cage shape and positive charge, which is realized by creating binary charge transfer complexes (Ta@Si_{16}^{+}–C_{60}^{-}) on the surfaces. The Ta@Si_{16} nanoclusters exhibit excellent thermal stability on C_{60}-teminated surfaces similar to those in the gas phase, whereas the nanoclusters destabilize at room temperature on 6T-terminated surfaces owing to the loss of electronic closure *via* a change in the charge state.

1 Introduction

The ability to create solid-state materials from atomic elements using a bottom-up method such as epitaxial growth, alloying, or chemical synthesis plays a crucial role in today's science and engineering. The controlled assembly of nanoclusters[1–9] is expected to be a novel material-processing methodology providing hierarchical nanostructures with tailored dimensionality and functionalities such as ultrathin heterojunctions exhibiting electrical rectification, photoelectric conversion, ferroelectricity, and high catalytic reactivity. Gas-phase-synthesized Si_{16} cages encapsulating a single metal atom (M@Si_{16}) are potential building blocks for such nanocluster assemblies, because their physicochemical properties are tunable while retaining the symmetrical cage shape by changing the type of metal atom and the charge state.[10–16] For instance, experimental and theoretical studies on M@Si_{16} nanoclusters in the gas phase have revealed that neutral Si_{16} cages including group-4 metals, such as Ti@Si_{16} and Zr@Si_{16}, behave as rare-gas-like superatoms because of their geometric and electronic shell closure,[10–15,17,18] whereas halogen- and alkali-like superatom characteristics emerge upon encapsulating metal atoms from group 3 (*e.g.* Sc@Si_{16} and Lu@Si_{16}) and group 5 (*e.g.* V@Si_{16} and Ta@Si_{16}), respectively.[13,14,18] Since their halogen- and alkali-like nature originates from the electronic open shell owing to the deficit and surplus of a single valence electron, they complete electron shells by adding and removing one electron, respectively.[13–18] These rare-gas-like M@Si_{16} anions and cations are selectively synthesized in the gas phase while exhibiting chemical and thermal stability.[13,14] Although this feature is advantageous for hierarchical nanostructuring on solid surfaces without losing the identity of each nanocluster building block, there is no knowledge about the properties, stability, and geometry of M@Si_{16} ions on solid surfaces.

The surface immobilization of M@Si_{16} ions without changing their original geometry and charge state is the key to M@Si_{16}-based nanostructuring. So far, the guiding principle for nondestructive nanocluster immobilization is a soft landing,[19–24] namely the deposition of cluster ions with sufficiently lower kinetic energy (E_k) than their interatomic binding energy. However, most nanocluster ions are neutral-

[a]*Nakajima Designer Nanocluster Assembly Project, ERATO, JST, KSP, 3-2-1 Sakado, Takatsu-ku, Kawasaki 213-0012, Japan. E-mail: nakajima@chem.keio.ac.jp*
[b]*Department of Chemistry, Faculty of Science and Technology, Keio University, 3-14-1 Hiyoshi, Kohoku-ku, Yokohama 223-8522, Japan*
[c]*Keio Institute of Pure and Applied Sciences (KiPAS), Keio University, 3-14-1 Hiyoshi, Kohoku-ku, Yokohama 223-8522, Japan*

†Electronic supplementary information (ESI) available. Effect of V_{tip} on the height of dots in STM images, deposition of Ta@Si_{16} cations with higher kinetic energy, and the theoretical optimization of geometries and electronic properties of Ta@Si_{16}–C_{60} complexes. See DOI: 10.1039/c4nr04211e

ized on conductive substrates in the conventional soft landing, which undesirably modifies their original properties. Our strategy toward overcoming this issue is to immobilize rare-gas-like $M@Si_{16}$ cations and anions on conductive surfaces functionalized with acceptor- and donor-like species, by which the positive and negative charges in the nanoclusters are expected to be retained by a donor–acceptor interaction,[25,26] respectively. In this study, we demonstrate by scanning tunneling microscopy and spectroscopy (STM/STS) that monolayers of $Ta@Si_{16}$ cations are formed by densely immobilizing $Ta@Si_{16}$ cations on conductive surfaces terminated with acceptor-like C_{60} molecules, in which each $Ta@Si_{16}$ nanocluster covalently connects to a single C_{60} molecule while maintaining the cage shape and positive charge by forming binary charge transfer complexes ($Ta@Si_{16}^{+}$–C_{60}^{-}). In contrast, $Ta@Si_{16}$ cations destabilize on metallic surfaces terminated with donor-like α-sexithiophene (referred to as 6T) molecules owing to the loss of electronic closure *via* a change in the charge state.

2 Materials and methods

All experiments were carried out under vacuum conditions. Highly oriented pyrolytic graphite (HOPG), Si(111)7 × 7, and Si(111)$\sqrt{3}$ × $\sqrt{3}$R30°-Ag [referred to as Si(111)$\sqrt{3}$-Ag] were prepared as substrates. These substrates were functionalized with monolayered films of C_{60} and 6T molecules by respectively depositing these molecules at room temperature (RT) under ultrahigh vacuum (UHV). HOPG surfaces were cleaned by thermal annealing at 770 K in UHV prior to the deposition of molecules. Si(111)$\sqrt{3}$-Ag surfaces were prepared by depositing 1 ML (7.83×10^6 atoms μm^{-2}) of Ag atoms on a Si(111)7 × 7 surface at 873 K. C_{60} molecules were deposited at RT by the thermal evaporation of C_{60} powder (purity: 99.95%) from a Ta crucible while maintaining a deposition rate of 0.03 ML min^{-1}, where 1 ML of C_{60} corresponds to 1.15×10^6 molecules μm^{-2}. 6T molecules were also deposited at RT by the thermal evaporation of 6T powder from a Ta crucible while maintaining a deposition rate of 0.015 ML min^{-1}, where 1 ML of 6T molecules corresponds to 0.62×10^6 molecules μm^{-2}.

Ta_nSi_m nanoclusters with various charge states were produced in gas aggregation apparatus with a direct-current magnetron sputtering source[27,28] from a Ta–Si mixed target. $Ta@Si_{16}$ cations were selectively created by the fine-tuning of synthesis conditions, similar to previous studies using the laser vaporization method.[13,14] The $Ta@Si_{16}$ cations were mass-selected from the cationic Ta_nSi_m species using a quadrupole mass spectrometer and were deposited onto substrates at ~90 K with a typical deposition rate of $\sim 2.6 \times 10^3$ ions μm^{-2} min^{-1}. E_k for the $Ta@Si_{16}$ cations was controlled to as low as possible by applying an appropriate positive voltage to the substrate during the deposition. The samples were transferred into an analysis chamber while maintaining the vacuum condition and were evaluated by STM/STS at RT under UHV.

3 Results and discussion

Fig. 1a and b respectively show wide- and molecular-scale STM images of a C_{60}/HOPG surface obtained after depositing a small amount of $Ta@Si_{16}$ cations with an E_k of ~0.01 eV per atom. Dot-shaped structures were uniformly created on the surface. The surface was densely covered with dots by continuously depositing cations for a long period (Fig. 1c). Our results indicate that each dot corresponds to an individual $Ta@Si_{16}$ nanocluster, as discussed below. In the histogram of dot heights (h_d) measured for the high-density dots (Fig. 1f), a peak appears at a h_d of ~0.8 nm. This value is close to the theoretical size of isolated $Ta@Si_{16}$ cations, which lies in the range of 0.89–0.95 nm for the isomers with C_{3v} and D_{4d} symmetry (Fig. 1e). Although the values of h_d shown in Fig. 1 were measured from STM height profiles obtained at a tip bias

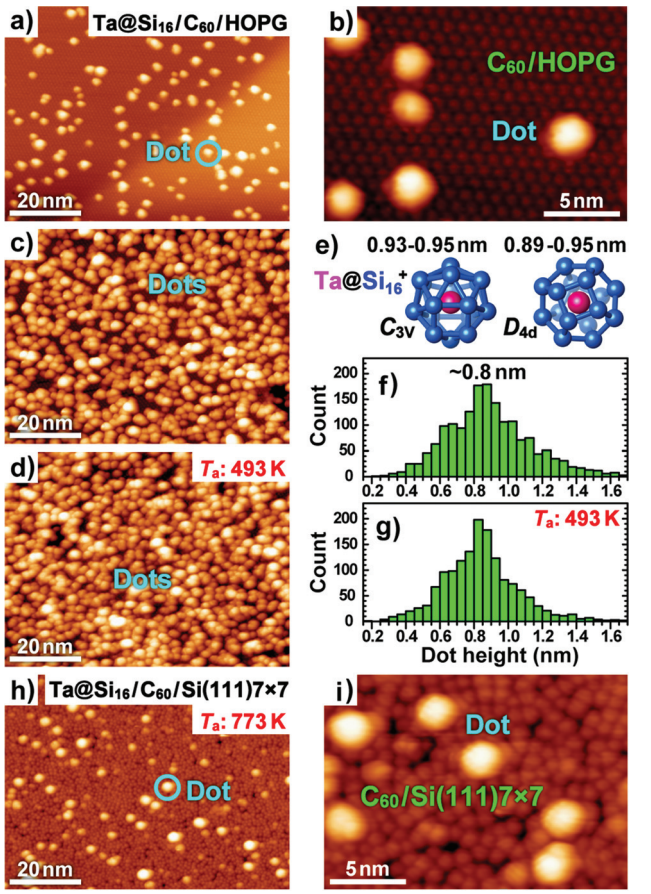

Fig. 1 Stable immobilization of $Ta@Si_{16}$ nanoclusters onto C_{60}-terminated surfaces. (a)–(d) STM images of C_{60}/HOPG surfaces obtained after depositing $Ta@Si_{16}$ cations. (a) Wide- and (b) molecular-scale images obtained after the initial deposition. (c) and (d) Surfaces densely covered with dots before and after annealing at 493 K, respectively. (e) Geometrical models and sizes of C_{3v} and D_{4d} isomers of $Ta@Si_{16}$ cations. (f) and (g) Histograms of the dot heights measured in (c) and (d), respectively. (h) Wide- and (i) molecular-scale STM images of the $Ta@Si_{16}^{+}$-deposited C_{60}/Si(111)7 × 7 surface obtained after annealing at 773 K. The imaging conditions (V_{tip} and I_t) are −2.3 V and 2 pA for (a)–(d), 2.2 V and 5 pA for (h), and 1.8 V and 5 pA for (i).

voltage (V_{tip}) of −2.3 V, the typical h_d of ~0.8 nm does not change with the value of the negative V_{tip} (see section 1 in the ESI†). The dots larger than the theoretical cluster size are considered to originate from the direct adsorption of $Ta@Si_{16}$ cations onto preexisting nanoclusters. On the other hand, the formation of smaller dots with h_d < 0.8 nm is attributed to the diversity in the adsorption sites of $Ta@Si_{16}$ nanoclusters. In a simple model using hard spheres with diameters of 1 nm for C_{60} molecules and 0.95 nm for $Ta@Si_{16}$ nanoclusters, the apparent heights of $Ta@Si_{16}$ nanoclusters adsorbed on the hollow and bridge sites in the C_{60} film are ~0.19 and ~0.14 nm lower than those on the atop sites, respectively. In fact, there is a small peak at h_d ~ 0.6 nm in the height histogram (Fig. 1f). Note that even smaller dots with h_d < 0.45 nm were dominantly created by depositing $Ta@Si_{16}$ cations with an intentionally larger E_k of ~1.25 eV per atom (Fig. S3a and S3b†), which is considered to come from the deformation and/or fragmentation of $Ta@Si_{16}$ nanoclusters on the surface, because such small values of h_d cannot be explained by the adsorption of $Ta@Si_{16}$ nanoclusters. These small dots are minor products in the current deposition, as shown in Fig. 1f. These results suggest that the $Ta@Si_{16}$ cations are immobilized without marked disintegration, which is further supported by evaluating the thermal stability and electronic structure of the dots.

Fig. 1d shows an STM image obtained after annealing the surface shown in Fig. 1c at 493 K. No marked changes in the density and spatial distribution of the dots were induced by annealing. In addition, there was no obvious change in the dot height distribution after the annealing, as confirmed from the height histograms measured before and after the annealing (Fig. 1f and 1g, respectively). To examine the thermal stability at higher temperatures, $Ta@Si_{16}$ cations were deposited onto a C_{60}-terminated Si(111)7 × 7 surface. This surface has high thermal durability owing to the covalent bonding between C_{60} molecules and the Si(111)7 × 7 surface,[29] while C_{60} molecules start to desorb from HOPG surfaces at ~510 K. Surprisingly, the dots remained after high-temperature annealing at 773 K (Fig. 1h and i).

The high thermal stability of the adsorbates on C_{60} films is consistent with the robust cage structure of $Ta@Si_{16}$ cations with an interatomic binding energy of ~4.45 eV.[16] In addition, the present results strongly indicate that the thermally activated diffusion and desorption of the adsorbate are inhibited by the strong adsorbate-C_{60} interaction compared with pure van der Waals forces. This consideration provides us with a reasonable explanation for the reduced typical dot height (~0.8 nm) compared with the theoretical size of isolated $Ta@Si_{16}$ cations (0.89–0.95 nm). The reduction of ~0.1 nm is similar to the difference between the van der Waals radius of Si atoms (0.211 nm) and the covalent radius in the Si–C bond (*e.g.* 0.094 nm in SiC crystals). In other words, a binary complex is locally created by the covalent bonding between the $Ta@Si_{16}$ nanocluster and the C_{60} molecule. Fig. 2 shows three theoretical motifs of neutral Ta@Si–C_{60} complexes (see section 3 in the ESI†). $Ta@Si_{16}$ nanoclusters are interconnected with

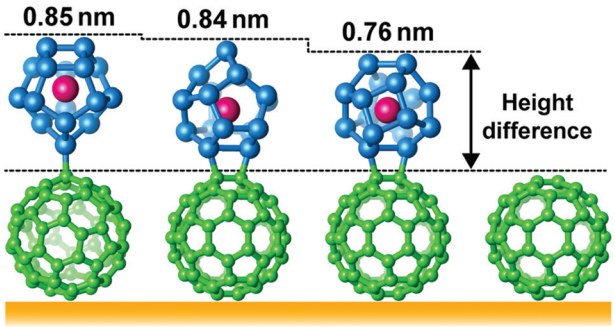

Fig. 2 Examples of theoretical motifs of neutral $Ta@Si_{16}$–C_{60} complexes.

each C_{60} molecule *via* one or two covalent bonds without impairing the cage shape. The theoretical height differences between $Ta@Si_{16}$ nanoclusters and C_{60} molecules are within the range of 0.76–0.85 nm, in good agreement with the typical dot height. Further evidence for such one-to-one covalent connection between $Ta@Si_{16}$ nanoclusters and C_{60} molecules is given as follows. It has been found that $Ta@Si_{16}$ nanoclusters change their adsorption position from the bridge or hollow sites to atop sites when C_{60} films sparsely covered with $Ta@Si_{16}$ nanoclusters (*e.g.*, Fig. 1a) are thermally annealed. Although the one-to-one covalent connection allows the $Ta@Si_{16}$ nanocluster to locally change their position among the neighboring adsorption sites *via* thermally activated precessional motion, it is considered to hardly occur for $Ta@Si_{16}$ nanoclusters covalently connected to multiple C_{60} molecules at bridge and atop sites; in other words, our result suggests that $Ta@Si_{16}$–$(C_{60})_2$ and $Ta@Si_{16}$–$(C_{60})_3$ are minor products.

The stability of the deposited $Ta@Si_{16}$ cations strongly depends on the surface. Fig. 3a shows an STM image of a 6T-terminated Si(111)$\sqrt{3}$-Ag surface obtained after the initial

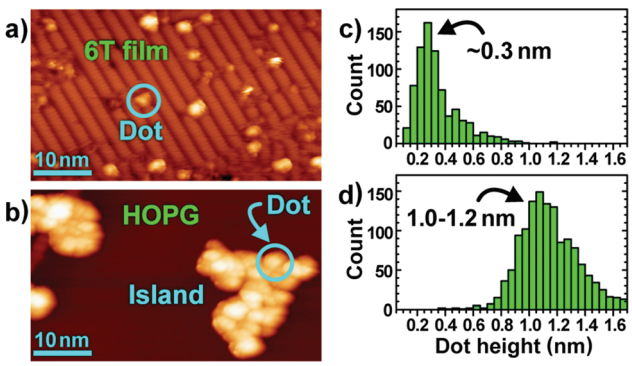

Fig. 3 Destabilization of $Ta@Si_{16}$ cations on surfaces. STM images obtained after initial deposition of $Ta@Si_{16}$ cations on (a) 6T/Si(111)$\sqrt{3}$-Ag and (b) HOPG surfaces. The imaging conditions (V_{tip} and I_t) are −1.6 V and 5 pA for (a) and −2.2 V and 2 pA for (b). (c) and (d) Histograms of dot heights measured on surfaces similar to those shown in (a) and (b), respectively. The dot heights in (c) were measured from STM line profiles obtained at various V_{tip} values of +1.7 V, −1.4 V, −1.5 V, −1.6 V, −1.8 V, and −2.0 V. The dot heights in (d) were measured from STM line profiles obtained at V_{tip} of −2.0 V and −2.2 V.

deposition of $Ta@Si_{16}$ cations. Small dots with a h_d of ~0.3 nm are created, as shown in the STM image and the dot-height histogram (Fig. 3c). This value does not sensitively fluctuate with the value of V_{tip} (see section 1 in the ESI†) and is close to the size of a single Si atom covalently bound with the surface, suggesting that the deposited $Ta@Si_{16}$ cations disintegrate into atoms and react with the 6T-teminated surface. Similar disintegration has been reported for Ag_{309} nanoclusters immobilized onto C_{60} monolayers formed on Au(111) surfaces, which is induced by the attractive force acting between the Ag_{309} nanoclusters and the substrate.[23] On the other hand, islands of dots with a disordered arrangement are formed by depositing $Ta@Si_{16}$ cations on HOPG surfaces (Fig. 3b). The height histogram of the dots/HOPG has the main peak at a h_d of 1.0–1.2 nm (Fig. 3d), suggesting that the marked disintegration of $Ta@Si_{16}$ nanoclusters, as observed on 6T/Si(111)$\sqrt{3}$-Ag, does not occur. However, the disordered arrangement of dots/HOPG is not improved by annealing, at least up to 493 K, also suggesting that the $Ta@Si_{16}$ nanoclusters aggregate *via* a strong interaction such as covalent Si–Si bonding. These results strongly indicate that the chemical reactivity of $Ta@Si_{16}$ cations is much greater on the 6T/Si(111)$\sqrt{3}$-Ag and HOPG surfaces than in the gas phase[13,14] and on C_{60}-terminated surfaces. The thermal and chemical stability of rare-gas-like $M@Si_{16}$ ions in the gas phase are interlinked with their simultaneous shell closure in the geometric and electronic structures.[10–18] Considering that the geometrical destruction of nanoclusters upon their collision with surfaces hardly occurs in the soft-landing scheme, particularly for the present deposition with a small E_k of ~0.01 eV per atom, the observed destabilization of $Ta@Si_{16}$ cations may be triggered by the loss of electronic closure *via* a change in the charge state. Paradoxically, the excellent thermal stability of $Ta@Si_{16}/C_{60}$ implies that $Ta@Si_{16}$ cations were immobilized onto C_{60}-terminated surfaces while retaining their charge state, which is supported by the following STS results.

Fig. 4a and b show normalized dI/dV spectra recorded on dot/6T and dot/HOPG surfaces, such as those shown in Fig. 3a and 3b, respectively. Positive and negative V_{tip} correspond to the filled and empty states of samples, respectively. In these spectra, peaks of the electronic density of states (DOS) appear near the Fermi level (E_F; V_{tip} = 0 V), as indicated by black arrows. The peak separations of ~0.6 eV for dot/6T and ~0.7 eV for dot/HOPG are clearly smaller than the theoretical energy gap between the highest occupied molecular orbital (HOMO) and the lowest unoccupied molecular orbital (LUMO) of isolated $Ta@Si_{16}$ cations (2.44 and 1.76 eV for C_{3v} and D_{4d} isomers,[16] respectively). In contrast, the spectrum recorded on dot/C_{60} with a h_d of 0.76 nm shows a large energy gap of ~2.1 eV between DOS peaks P_1 and P_2 (Fig. 4c), which is close to the theoretical HOMO–LUMO gap of the isolated $Ta@Si_{16}$ cations. Note that HOMO–LUMO gaps in dI/dV spectra are sometimes measured to be larger than the actual values, because Coulomb repulsion and attraction *via* electron and hole injections sometimes locally increase and decrease the potential energy of samples, respectively.[30,31] However,

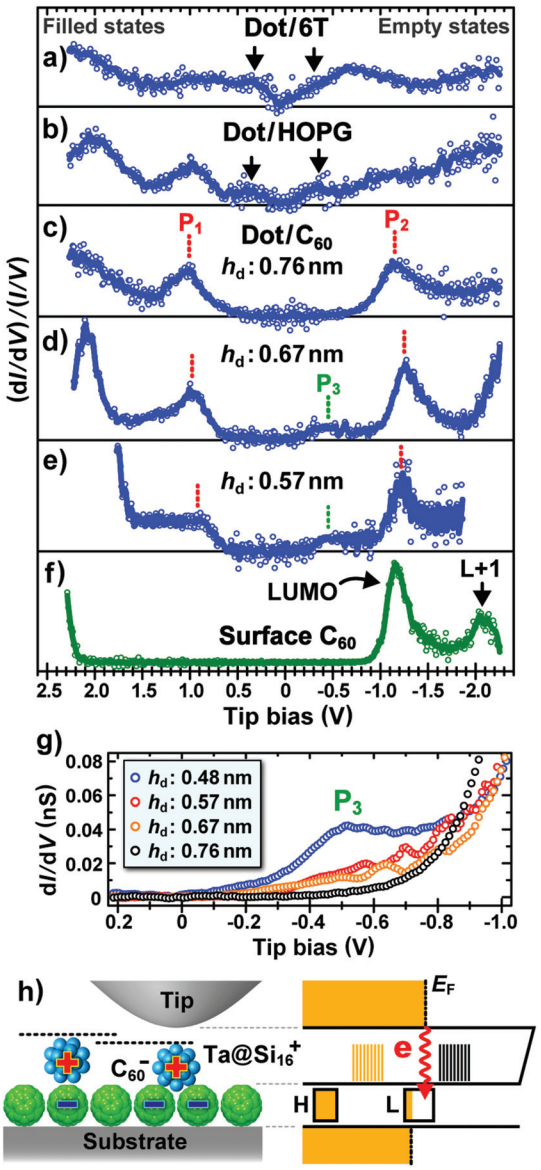

Fig. 4 Electronic structures of $Ta@Si_{16}$/surfaces. Normalized dI/dV spectra measured on (a) dot/6T, (b) dot/HOPG, (c)–(e) dots/C_{60}, and (f) bare C_{60} molecules. (g) Series of non-normalized dI/dV spectra of dots/C_{60} with various h_d values, which are focused to investigate the behavior of P_3. Each dI/dV datum was numerically derived from the respective tunneling I–V curve obtained by averaging almost 100 original curves. The set points (V_{tip} and I_t) of the I–V measurements were –1.5 V and 80 pA for (a), –1.9 V and 80 pA for (b), and –1.4 V and 150 pA for (c)–(f). (h) Schematic potential diagram of the tip/gap/$Ta@Si_{16}^{+}/C_{60}^{-}$/substrate junction.

such an increase in the energy gap is greatly suppressed in STS measurements of adsorbates strongly bound with a surface, such as $Ta@Si_{16}$ nanoclusters deposited on 6T- and C_{60}-terminated surfaces. Actually, a small energy gap of ~0.6 eV is observed for dot/6T as shown in Fig. 4a. Furthermore, the difference in the energy gaps shown in Fig. 4a–c is qualitatively explained by the geometry and static charge state of $Ta@Si_{16}$ nanoclusters on surfaces without considering the energy-

gap modification in the STS measurements, as discussed next.

The large HOMO–LUMO gap of rare-gas-like M@Si_{16} ions originates from both the highly symmetrical coordination of Si atoms around the central metal atom and the arrangement of valence electrons with jellium-like electronic shells.[10–18] In contrast, the energy gap of M@Si_{16} ions markedly decreases upon deformation into low-symmetry isomers[15,16] and their interconnection *via* covalent Si–Si bonds.[32] On the other hand, it is also predicted that the electronic structure of M@Si_{16} ions is modified by simply changing their charge state.[11,12] For instance, when a single extra electron is statically injected into rare-gas-like neutral Ti@Si_{16} nanoclusters, an occupied molecular orbital appears near E_F after the splitting of the original electronic state.[11] Although similar phenomena should occur in neutralized Ta@Si_{16} cations, the STS spectrum of Ta@Si_{16}/C_{60} exhibits a large energy gap between the two DOS peaks that appear at much higher and lower energies than E_F, suggesting that the deposited Ta@Si_{16} cations retain not only their cage shape but also their cationic state on C_{60} films. Here, since we have observed that a positive current was the output from the substrates during the deposition of Ta@Si_{16} cations, it is considered that the cation is first neutralized immediately after adsorption by the injection of an electron from the substrate and then cationized again by the donation of an electron into the underlying C_{60} molecule. This is supported by the results of a theoretical calculation: Ta@Si_{16} nanoclusters and C_{60} molecules in the complexes shown in Fig. 2 tend to be positively and negatively charged *via* spontaneous polarization, respectively (Table S1†).

Actually, the electron transfer from Ta@Si_{16} nanoclusters to C_{60} molecules in the Ta@Si_{16}/C_{60} system is observed in the following results. Fig. 4d and 4e show the normalized dI/dV spectra measured on slightly shorter dots with a h_d of 0.67 and 0.57 nm, respectively. Comparing Fig. 4c–e, the positions of peaks P_1 and P_2 are constant regardless of the value of h_d, which is consistent with the preceding consideration that the variation of h_d in the range of 0.55–0.85 nm is not due to the deformation of the Ta@Si_{16} nanoclusters themselves but due to their position on the C_{60} film. In contrast, an additional peak P_3 with low intensity is observed near E_F for the shorter dots. A possible origin of P_3 is the molecular orbital of the underlying C_{60} molecule, which can be measured using STS by directly injecting tunneling electrons into the C_{60} molecule within the energy gap of the Ta@Si_{16} nanocluster, as schematically shown in Fig. 4h. However, its contribution to the tunneling conductance should be smaller for taller dots because of the increased tip–C_{60} distance. This feature is indeed observed in the non-normalized dI/dV spectra focused on P_3 (Fig. 4g), in which the intensity of P_3 decreases with increasing h_d. Here, on C_{60} molecules located sufficiently far from dots, the LUMO appears at 1.2 eV above E_F (Fig. 4f), indicating their charge neutrality.[33,34] In contrast, the LUMO of C_{60} molecules is known to be markedly lowered and appear slightly above E_F by donating electrons from chemically doped alkali-metal atoms[35] or from metallic surfaces.[30,33] The present STS results suggest that similar charge transfer occurs in the Ta@Si_{16}/C_{60} system immediately after the neutralization of Ta@Si_{16} cations, which is consistent with the fact that neutral Si_{16} cages encapsulating a group-5 metal atom (*e.g.* V@Si_{16} and Ta@Si_{16}) exhibit alkali-like characteristics.[13–15]

4 Conclusions

In summary, we have demonstrated that the successful immobilization of gas-phase-synthesized Ta@Si_{16} cations onto C_{60}-terminated surfaces *via* a donor–acceptor interaction while maintaining their cage shape and positive charge. This has enabled us to form a heterojunction exhibiting spontaneous polarization from two types of monolayers of superatomic Ta@Si_{16} cations and C_{60} anions. Such an ultrathin heterojunction would be useful for the charge separation layers in nanoscale devices such as capacitors and photovoltaic cells. Furthermore, the present results also suggest that the controlled immobilization of nanocluster ions exhibiting various charge states would be possible by controlling the donor–acceptor interaction between the nanoclusters and the surface, which is expected to play a key role in the design of high-performance catalysts, because it is known that the charge state of supported nanoclusters is a key factor in promoting their catalytic reactivity.[36] A novel avenue for developing nanocluster-based materials science and technology is thus open to us.

Notes and references

1 S. N. Khanna and P. Jena, *Phys. Rev. Lett.*, 1992, **69**, 1664–1667.
2 S. B. Darling, N. A. Yufa, A. L. Cisse, S. D. Bader and S. J. Sibener, *Adv. Mater.*, 2005, **17**, 2446–2450.
3 Md. A. Alam, Y.-S. Kim, S. Ogawa, A. Tsuda, N. Ishii and T. Aida, *Angew. Chem., Int. Ed.*, 2008, **47**, 2070–2073.
4 S. A. Claridge, A. W. Castleman Jr., S. N. Khanna, C. B. Murray, A. Sen and P. S. Weiss, *ACS Nano*, 2009, **3**, 244–255.
5 A. W. Castleman Jr. and S. N. Khanna, *J. Phys. Chem. C*, 2009, **113**, 2664–2675.
6 T. Osuga, T. Murase and M. Fujita, *Angew. Chem., Int. Ed.*, 2012, **51**, 12199–12201.
7 X. Roy, C.-H. Lee, A. C. Crowther, C. L. Schenck, T. Besara, R. A. Lalancette, T. Siegrist, P. W. Stephens, L. E. Brus, P. Kim, M. L. Steigerwald and C. Nuckolls, *Science*, 2013, **341**, 157–160.
8 Y. H. Jang, K. Chung, L. N. Quan, B. Špačková, H. Šípová, S. Moon, W. J. Cho, H.-Y. Shin, Y. J. Jang, J.-E. Lee, S. T. Kochuveedu, M. J. Yoon, J. Kim, S. Yoon, J. K. Kim, D. Kim, J. Homola and D. H. Kim, *Nanoscale*, 2013, **5**, 12261–12271.

9 J. M. Pettibone, W. A. Osborn, K. Rykaczewski, A. A. Talin, J. E. Bonevich, J. W. Hudgens and M. D. Allendorf, *Nanoscale*, 2013, **5**, 6558–6566.
10 V. Kumar and Y. Kawazoe, *Phys. Rev. Lett.*, 2001, **87**, 045503.
11 H. Kawamura, V. Kumar and Y. Kawazoe, *Phys. Rev. B: Condens. Matter*, 2005, **71**, 075423.
12 J. U. Reveles and S. N. Khanna, *Phys. Rev. B: Condens. Matter*, 2006, **74**, 035435.
13 K. Koyasu, M. Akutsu, M. Mitsui and A. Nakajima, *J. Am. Chem. Soc.*, 2005, **127**, 4998–4999.
14 J. Atobe, K. Koyasu, S. Furuse and A. Nakajima, *Phys. Chem. Chem. Phys.*, 2012, **14**, 9403–9410.
15 M. B. Torres, E. M. Fernández and L. C. Balbás, *Phys. Rev. B: Condens. Matter*, 2007, **75**, 205425.
16 H. Cantera-López, L. C. Balbás and G. Borstel, *Phys. Rev. B: Condens. Matter*, 2011, **83**, 075434.
17 J. T. Lau, K. Hirsch, Ph. Klar, A. Langenberg, F. Lofink, R. Richter, J. Rittmann, M. Vogel, V. Zamudio-Bayer, T. Möller and B. von Issendorff, *Phys. Rev. A*, 2009, **79**, 053201.
18 P. Jena, *J. Phys. Chem. Lett.*, 2013, **4**, 1432–1442.
19 K. Bromann, C. Félix, H. Brune, W. Harbich, R. Monot, J. Buttet and K. Kern, *Science*, 1996, **274**, 956–958.
20 V. N. Popok, I. Barke, E. E. B. Campbell and K.-H. Meiwes-Broer, *Surf. Sci. Rep.*, 2011, **66**, 347–377.
21 K. A. Wepasnick, X. Li, T. Mangler, S. Noessner, C. Wolke, M. Grossmann, G. Ganteföer, D. H. Fairbrother and K. H. Bowen, *J. Phys. Chem. C*, 2011, **115**, 12299–12307.
22 B. Wang, B. Yoon, M. König, Y. Fukamori, F. Esch, U. Heiz and U. Landman, *Nano Lett.*, 2012, **12**, 5907–5912.
23 S. Duffe, N. Grönhagen, L. Patryarcha, B. Sieben, C. Yin, B. von Issendorff, M. Moseler and H. Hövel, *Nat. Nanotechnol.*, 2010, **5**, 335–339.
24 M. Nakaya, T. Iwasa, H. Tsunoyama, T. Eguchi and A. Nakajima, *Adv. Funct. Mater.*, 2014, **24**, 1202–1210.
25 E. Mena-Osteritz and P. Bäuerle, *Adv. Mater.*, 2006, **18**, 447–451.
26 L. Chen, W. Chen, H. Huang, H. L. Zhang, J. Yuhara and A. T. S. Wee, *Adv. Mater.*, 2008, **20**, 484–488.
27 H. Tsunoyama, C. Zhang, H. Akatsuka, H. Sekiya, T. Nagase and A. Nakajima, *Chem. Lett.*, 2013, **42**, 857–859.
28 C. Zhang, H. Tsunoyama, H. Akatsuka, H. Sekiya, T. Nagase and A. Nakajima, *J. Phys. Chem. A*, 2013, **117**, 10211–10217.
29 K. Sakamoto, M. Harada, D. Kondo, A. Kimura, A. Kakizaki and S. Suto, *Phys. Rev. B: Condens. Matter*, 1998, **58**, 13951–13956.
30 X. Lu, M. Grobis, K. H. Khoo, S. G. Louie and M. F. Crommie, *Phys. Rev. B: Condens. Matter*, 2004, **70**, 115418.
31 I. F. Torrente, K. J. Franke and J. I. Pascual, *J. Phys.: Condens. Matter*, 2008, **20**, 184001.
32 M. B. Torres, E. M. Fernández and L. C. Balbás, *J. Phys. Chem. C*, 2011, **115**, 335–350.
33 M. Nakaya, Y. Kuwahara, M. Aono and T. Nakayama, *Small*, 2008, **4**, 538–541.
34 M. Nakaya, Y. Kuwahara, M. Aono and T. Nakayama, *J. Nanosci. Nanotechnol.*, 2011, **11**, 2829–2835.
35 M. S. Dresselhaus, G. Dresselhaus and P. C. Eklund, Classification and Structure of Doped Fullerenes, in *Science of Fullerenes and Carbon Nanotubes*, Academic Press, San Diego, CA, 1996, pp. 224–263.
36 B. Yoon, H. Häkkinen, U. Landman, A. S. Wörz, J.-M. Antonietti, S. Abbet, K. Judai and U. Heiz, *Science*, 2005, **307**, 403–407.